STRAIN ASSESSMENT IN USFOS

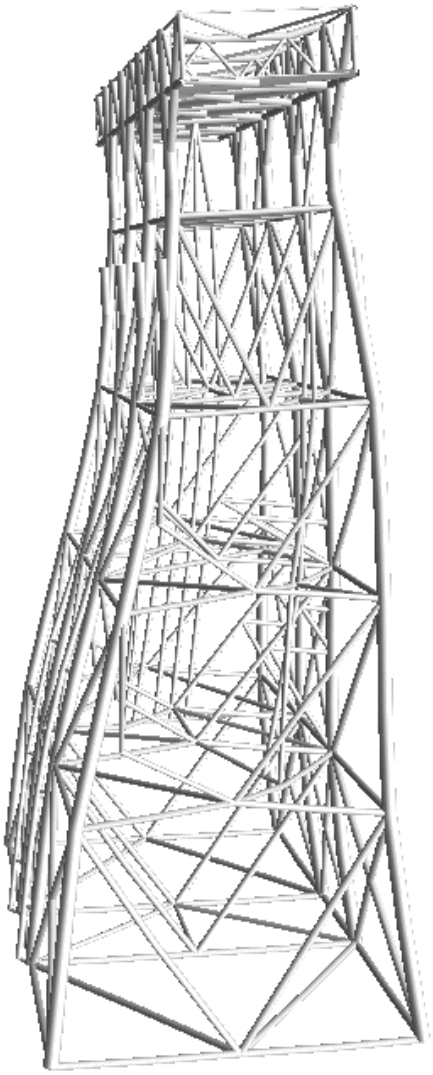

CONTENTS:

1 Introduction

The purpose of this model is to describe the revised strain calculation model in USFOS. The strains obtained with the revised model are investigated for a few characteristic cases, including a case that has been analyzed with shell modeling and alternative software (ABAQUS, USFOS).

Recommendations for parameters to be used for calculations of strains are given.

2 Revised strain calculation model

The original strain calculation model is described in USFOS theory manual and is recapped in Appendix. A weakness of the model is that it is based upon total plastic displacements and rotations. An important parameter is the hinge length, which depends on the moment distribution over the beam and the axial force level. With the present version a change in the moment distribution and the axial force has a direct impact on the strain, including the previous levels. This may for example cause a spurious reduction or increase of the strain during elastic unloading, in which case the strain should remain constant.

In order to overcome this problem an incremental approach is adopted. The total strains for two adjacent steps are calculated using the last updated values of the bending moments and axial force for the member.

Thus the strain at step no. i is estimated by the following algorithm:

$$\varepsilon_{\max,i} = \varepsilon_{\max,i-1} + \Delta\varepsilon_{\max,i}$$
$$\Delta\varepsilon_{\max,i} = \varepsilon_{\max}\left(\theta^{tot,i}, M_{1,i}, M_{2,i}, N_i\right) - \varepsilon_{\max}\left(\theta^{tot,i-1}, M_{1,i}, M_{2,i}, N_i\right)$$

With this procedure a change of the "cantilever" length (refer excerpt from theory manual in Appendix) will not have an intermediate impact on the strain level.

Furthermore, calculation of strains increments is not carried out if the total plastic rotation $\theta^{\square\square\square}$ is constant.

The "cantilever" length concept is very useful, in the sense that it is automatically adjusted when a mid hinge is introduced.

3 Strain predictions for various characteristic cases.

3.1 Beam with concentrated load at mid span

This example is highly relevant for ship collision problems. For simplicity only one element is modeled, a tubular member with the following data:

- Diameter D = 1m
- Thickness t = 60 mm
- Length L = 25 m
- Yield stress f_Y = 300 MPa
- Default hardening c = 0.002

The beam is modeled with clamped and axially fixed end so that ity will start by developing a three hinge bending mechanism, where the bending action is transformed in membrane action when the deformations become finite. The default modeling is 2 members with a concentrated load representing a collision load at mid span. To see the effect of element subdivision strains are also estimated using 6 elements as shown in Figure 3.1. The example with 2 elements is identical to the one discussed in Chapter 7.8 in *Nonlinear Analysis of Offshore Structures* by B. Skallerud and J. Amdahl (2002)

The load factor versus mid point displacement is shown in Figure 3.2.

The predicted maximum strain is plotted in the same diagram as Fig. 7.19 in the book and is redrawn in Figure 3.3. It shows that the revised model agrees very well with the old model, but avoids the spurious nonlinearity when hinges (quarter length) are formed. USFOS predictions are in good agreement with ABAQUS results and USFOS shell modeling. It is noteworthy to see that ABAQUS results depend considerably on mesh size. This is a well-known phenomenon in nonlinear finite element analysis.

The rapid increase in strain for a displacement of 0.2 m is due to the yield plateau assumed in the strain prediction model. It ceases when the strain reaches the level for onset of hardening.

Figure 3.4 shows a comparisons of strains predicted with 2 elements and 6 elements. The strains agree very well. Some small irregularities are observed for the 6-element model. They are due to small rotations caused by the large number of hinges that are produced, actually up to 15 hinges. The strain predictions demonstrate that use many small elements for the same geometry does not increase the accuracy and should be avoided. Otherwise, the results confirm that the procedure used to predict the hinge length works well.

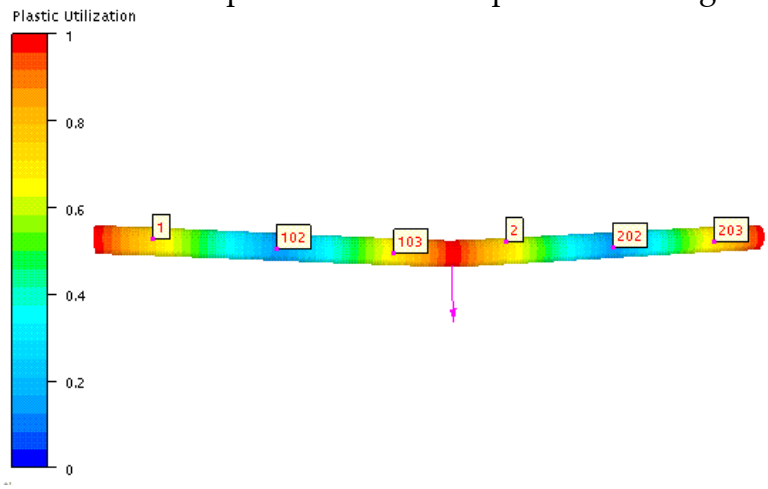

Figure 3.1 Beam modeled with six elements

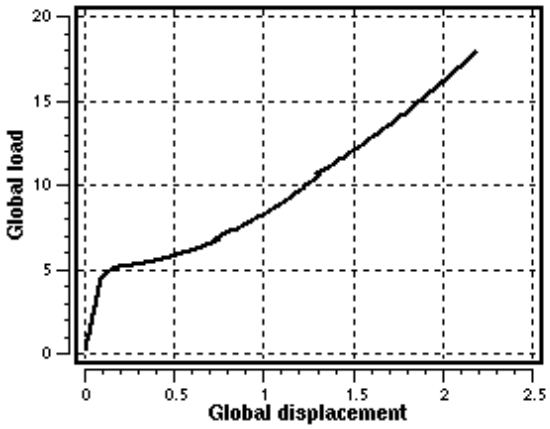

Figure 3.2 Global load versus lateral displacement for beam

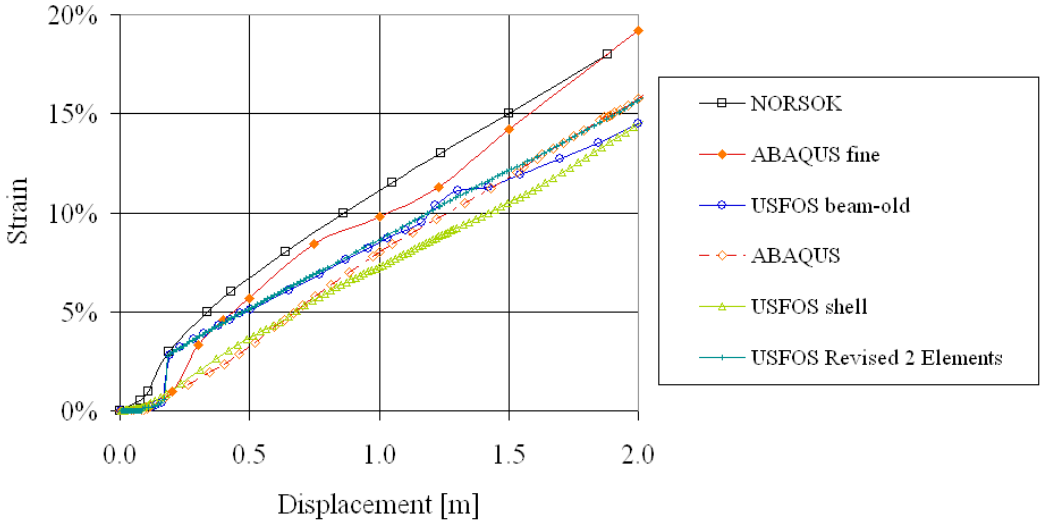

Figure 3.3 Maximum strain predictions in beam (Refer Skallerud & Amdahl: *Nonlinear Analysis of Offshore Structures*)

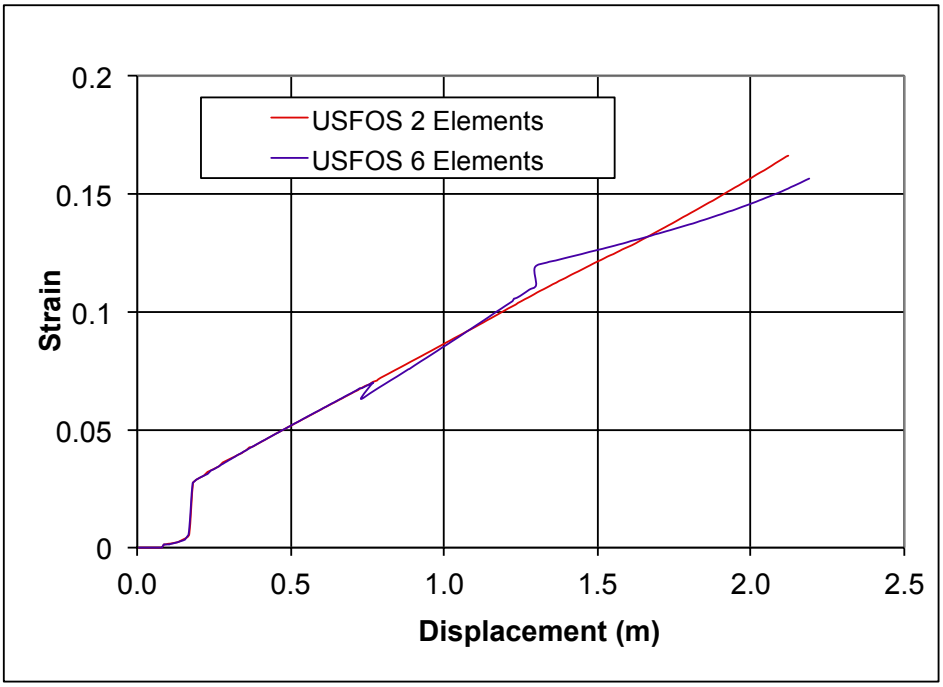

Figure 3.4 Maximum strain with 2 and 6 beam elements

3.2 Beam subjected to axial tension

This case is chosen because customers often perform test with the strain model using a simple tensile member. It is probably used because material

tests are performed with tension coupon specimens. The outcome of the test is engineering stress-strain relationships. It is emphasized that the example is "hypothetic" in the sense that a platform member never will experience pure tension, but will always be subjected to rotation which will contribute to localization of the strain.

The finite element model using 6 elements is shown in Figure 3.5. The load factor versus elongation is displayed in Figure 3.6. The response is initially elastic, followed by elasto-plastic transition to the strain hardening region.

The geometry and material data are the same as for the previous example.

Figure 3.7 shows the strains versus elongation using 1, 2, 3 and 6 element subdivisions, respectively. The strains agree very well regardless of the number of elements and confirm that the model works well for pure tension. The strain remains a smooth function also when mid hinges for the two elements are introduced at beam quarter lengths.

The average strain, obtained by smearing the elongation uniformly over the member, is also plotted. It is observed that a peak strain of 0.10 corresponds to an average strain of 0.03 and a peak strain of 0.15 to average strain of 0.05.

It is noticed that an average strain of 0.03 corresponds to onset of hardening for the assumptions used (yield plateau 20 x yield strain), so using a peak strain in the range of 0.10 to 0.15 is not unreasonable.

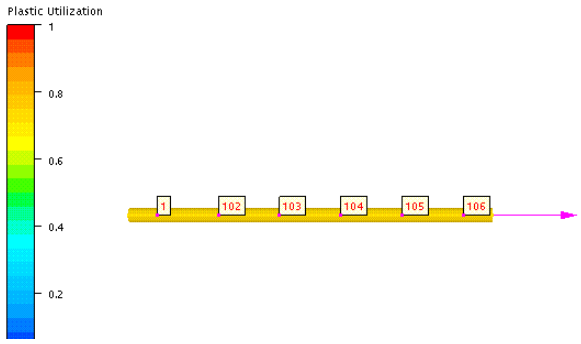

Figure 3.5 Tension member modeled with six elements

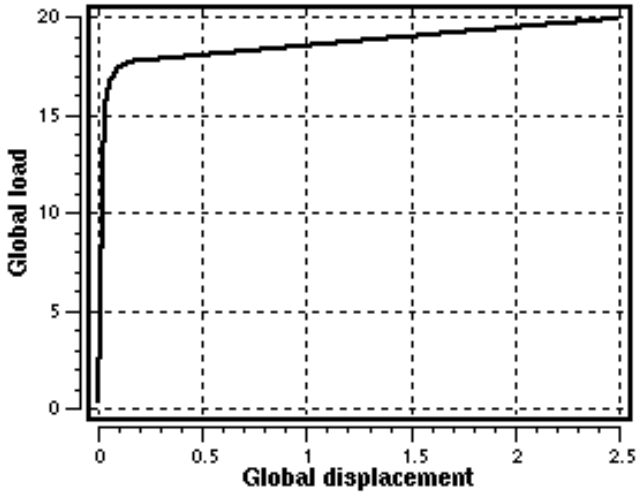

Figure 3.6 Global load versus elongation for tension member

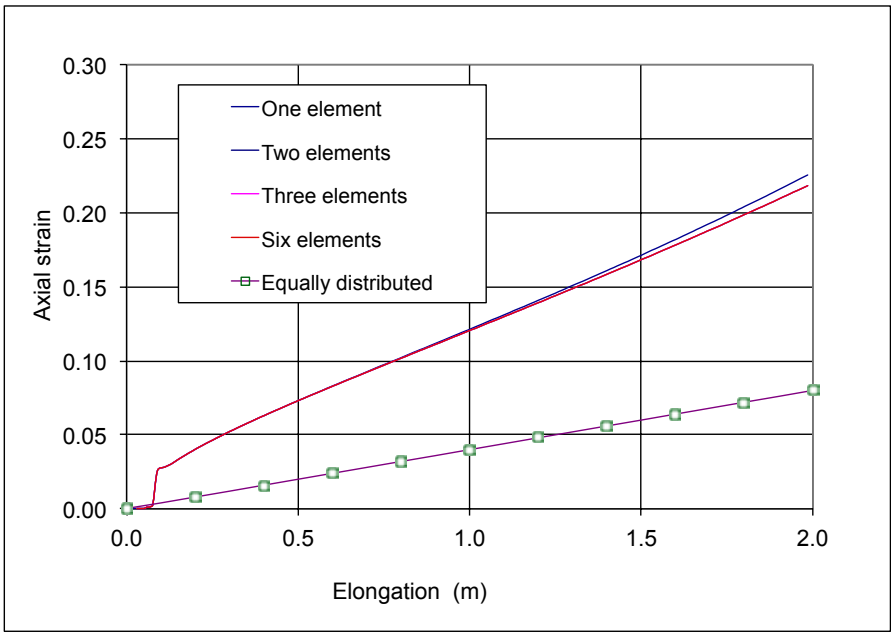

Figure 3.7 Strain versus elongation for various number of elements.

3.3 Brace tension member

This example is chosen because it simulates a behavior of an X-braced jacket. During progressive collapse tension braces will undergo significant elongation (in addition to some rotation). X-braced jackets are very redundant, as long as fracture is not initiated in the tension brace. Hence, it is essential to control that the strains do not become unacceptably large in the tension braces.

The model is the so-called Zayas frame (which can be found in USFOS/Examples folder).

The finite element model is shown in Figure 3.8. The behavior of tension brace- Element 1 – is focused. The member is modeled with 1, 2, 4, 6 and 8 sub-elements, respectively. Figure 3.8 shows the 6-element model (the REFINE option has been used to generate the model).

The global load versus lateral displacement is shown in Figure 3.9 and is virtually independent of element 1 subdivision.

The strain versus lateral displacement for all sub-elements for the various subdivisions is plotted in Figure 3.10 through Figure 3.14. The strain predictions are in the same range, but some variations are observed. This is due to the fact that the local rotations tend to play a larger role when the number of elements increases. Significant subdivision of the uniform member tends to destabilize the calculations.

Based on a fair judgment of strains – it may be argued that the critical strain o.15 is reached for a global displacement of 0.6 m with 1 element, 0.9 m for 2 elements, 0.8 m for 4 elements, 0.7 m for 6 elements and 0.6 m for 8 elements.

Inevitably some deviations exist; a fair estimate is probably to use 0.6 m as failure criterion.

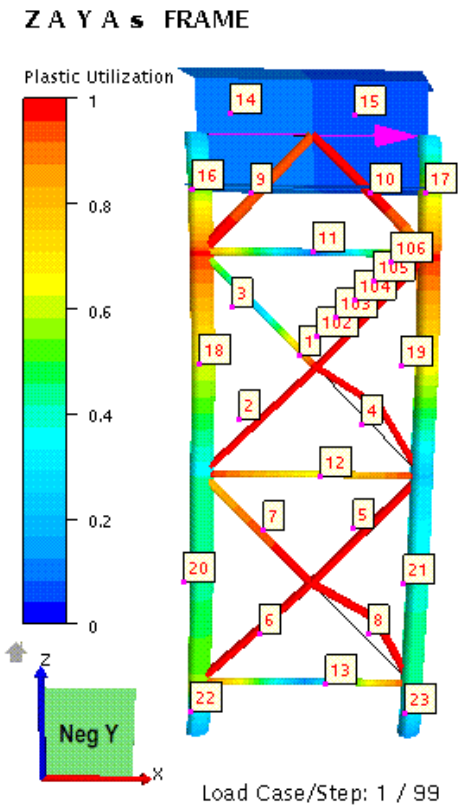

Figure 3.8 Frame model – tension diagonal 1, modeled with six elements: Element no´s 1, 102,103….106.

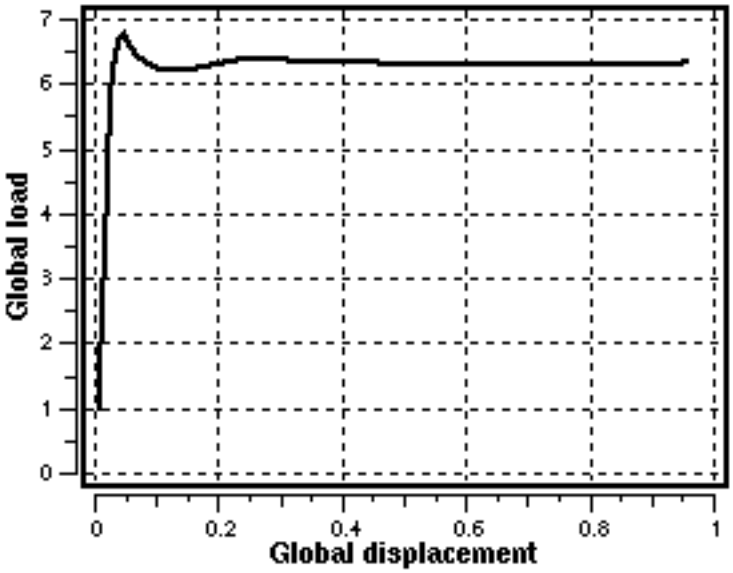

Figure 3.9 Global load versus lateral displacement for frame

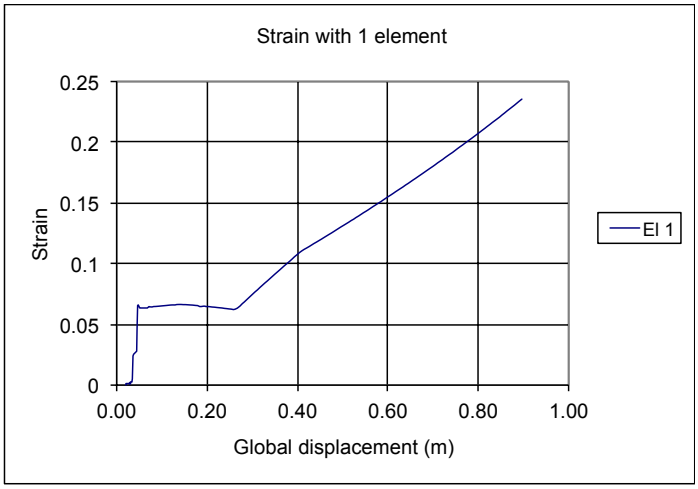

Figure 3.10 Strain in tension diagonal with 1 element

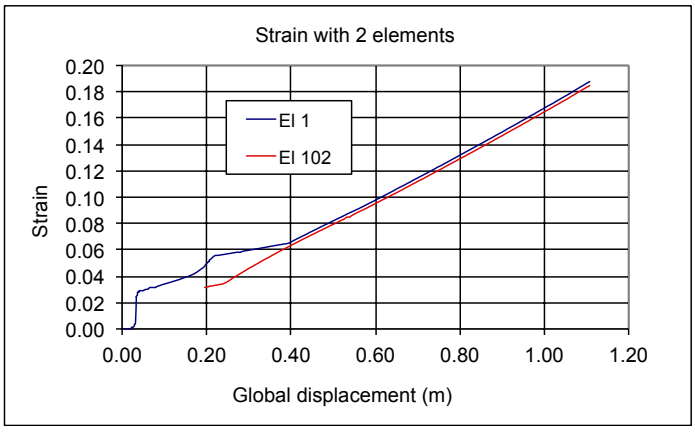

Figure 3.11 Strain in tension diagonal with 2 elements

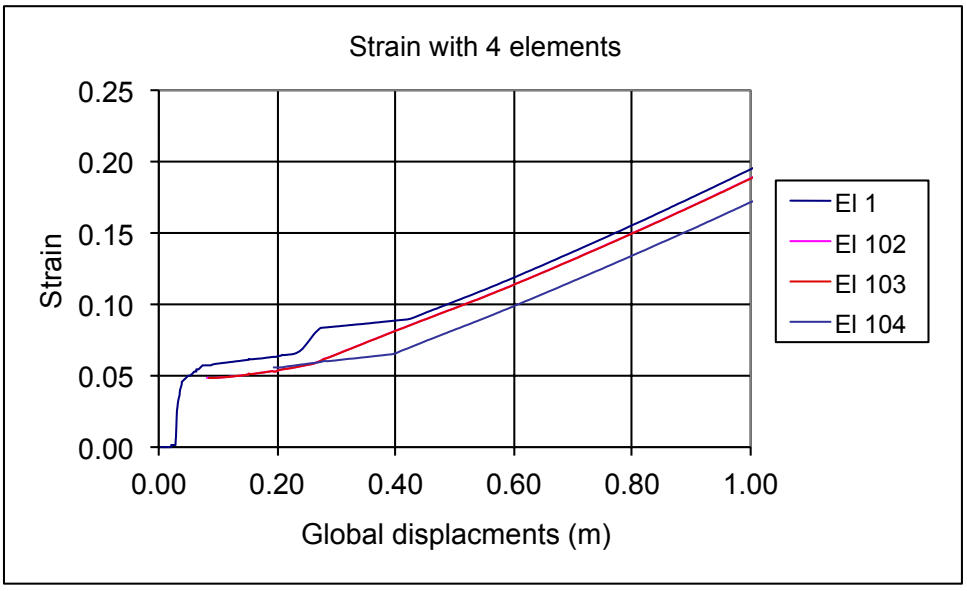

Figure 3.12 Strain in tension diagonal with 4 elements

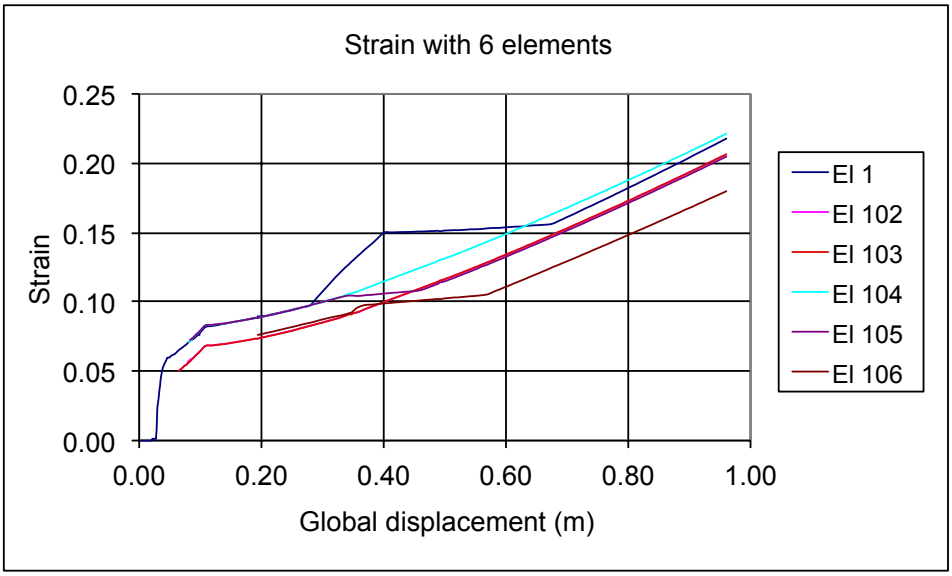

Figure 3.13 Strain in tension diagonal with 6 elements

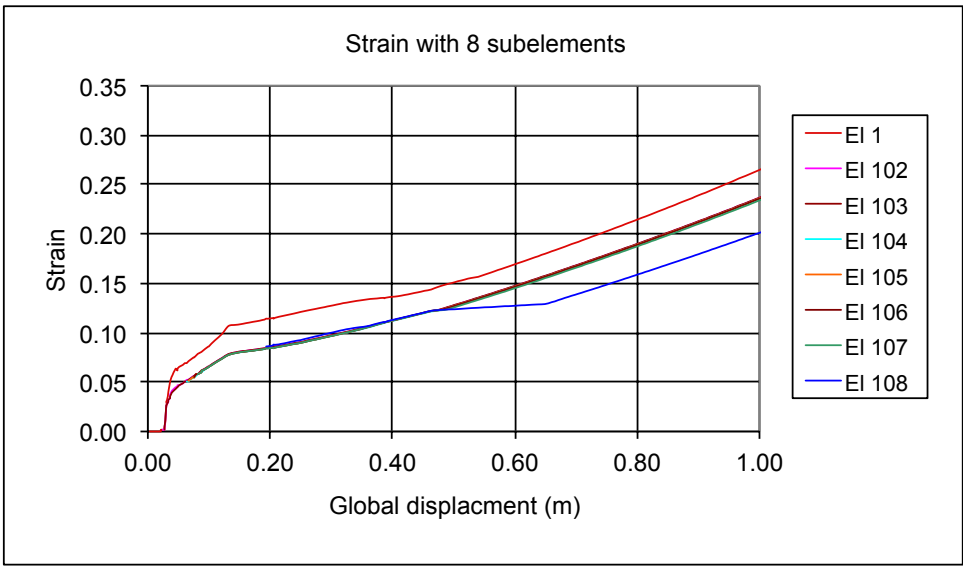

Figure 3.14 Strain in tension diagonal with 8 elements

3.4 Cyclic behavior

This section studies the behavior of the strain calculation module during cyclic loading. The structural model is the beam model from Section3.1. In the first case (1) the beam is unloaded to zero after reaching load factor 8.0. This simulates a collision case where the collision load is unloaded after the maximum energy is reached.

The second case (2) is more extreme, in the sense that the lateral load is reversed before returning to the original direction. Further, the strain for a uniform load is compared with that of a concentrated load.

3.4.1 Elastic unloading and reloading

The global load versus – global displacements for the two cases are shown Figure 3.15 and the corresponding strains in Figure 3.16. When unloading is performed at a global displacement of 1.0 the strain level remains constant, as it should. In case 1 the strain increases again when the displacement exceeds 1.0.

In case 2 the strain decreases as the load is reversed and becomes virtually zero. Upon reloading the strain follows the same track as case 1. In both cases the strains follows the path for monotonous load. The conclusion is that the strain procedure works excellently for cyclic loading.

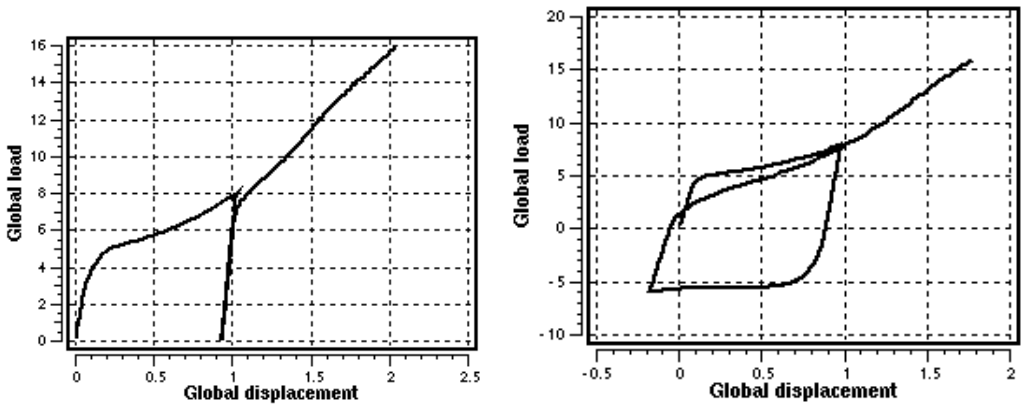

Case 1 Case 2

Figure 3.15 Global load versus global displacement for elastic unloading to zero (Case 1) and cyclic loading (Case 2)

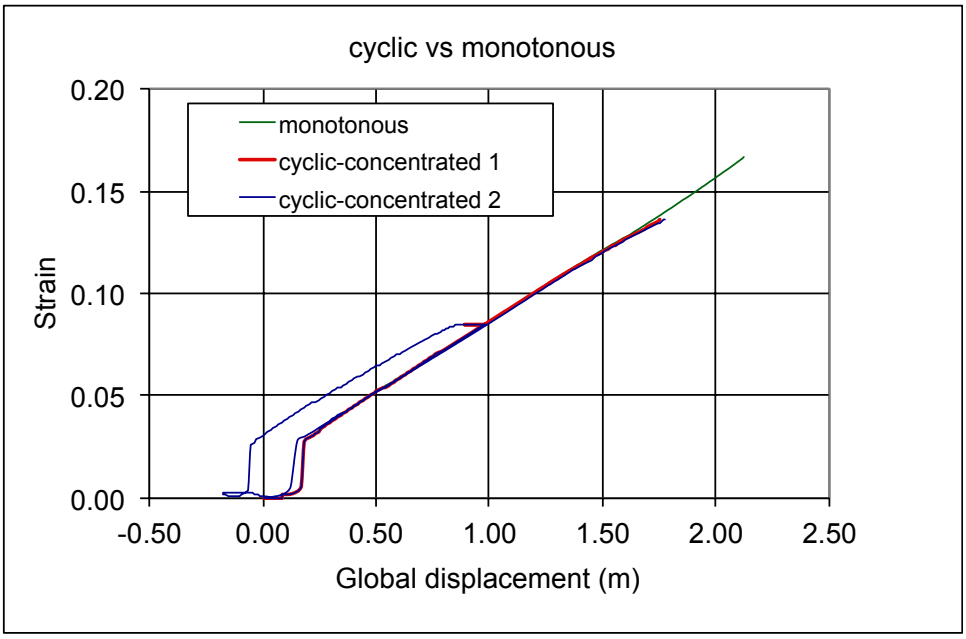

Figure 3.16 Strain versus global displacment

3.4.2 Distributed load versus concentrated load

The intensity of the uniform load is equal to □□=*2*□□/□□, so that the load factor at collapse is approximate the same as for the case with concentrated load. The strain history for case 1 is compared with that for concentrated load in Figure 3.17 and for case 2 in Figure 3.18. The strain histories show much of the same features when the load is distributed, but it increases more rapidly for large deformations. The slope increases in the first cycle takes place when mid hinges are introduced in each of the two elements (quarter length). This causes a smaller "cantilever" length. In addition the plastic rotations at the supports are larger for distributed load.

The strain of interest is the maximum tensile strain. For case 2 the point of maximum strain shifts form one side of the beam to the other. The explains the somewhat "odd" shape of the curves for negative global displacement in the case of distributed load.

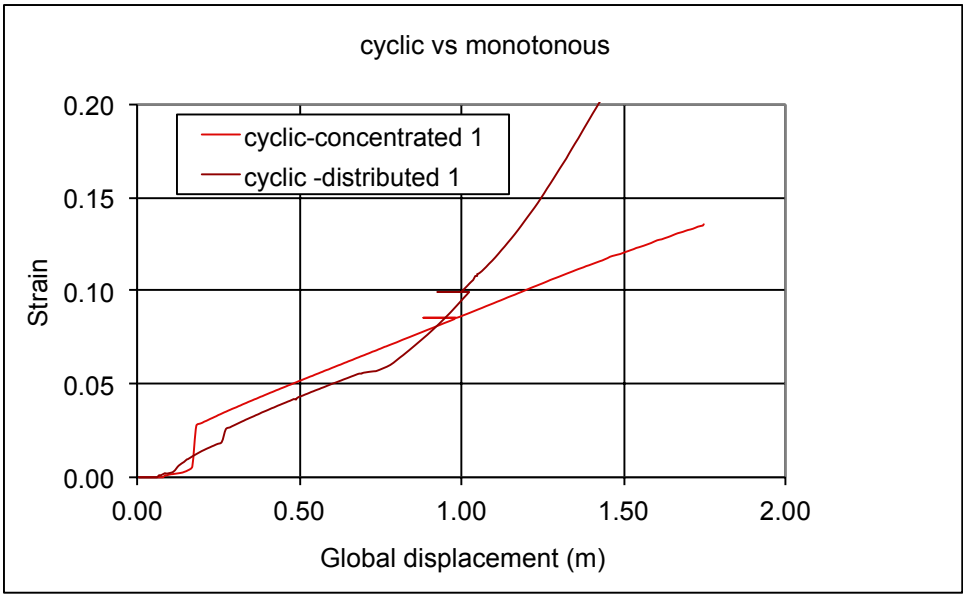

Figure 3.17 Strain versus global displacement case 1

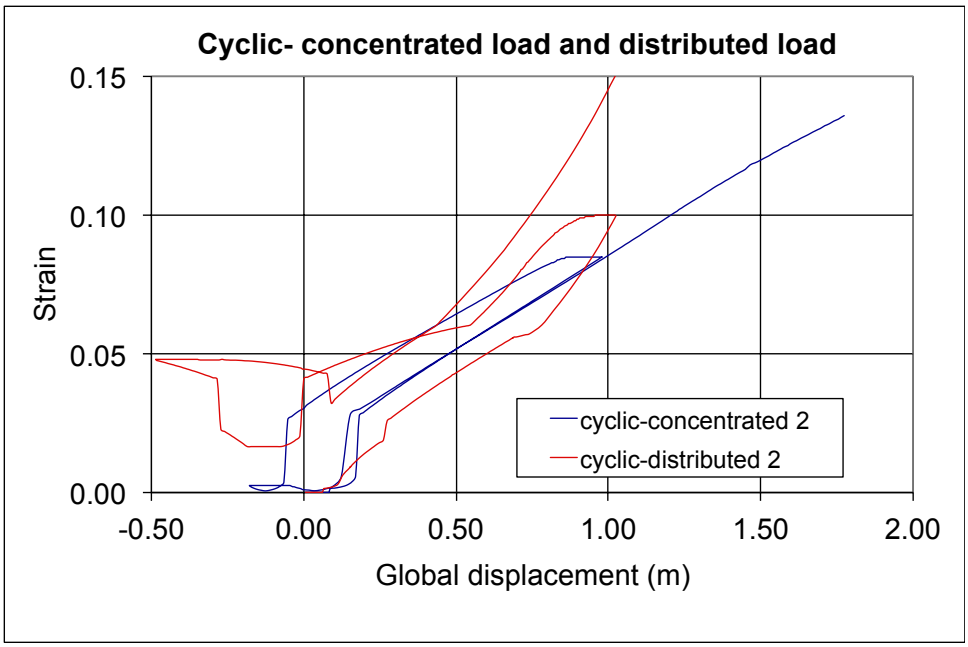

Figure 3.18 Strain versus global displacement case 2

3.5 Effect of local denting

The present example is concerned with the effect of local denting on strain predictions. This is particularly relevant for ship collision problems. ship collision problems. The example is similar to that of Section 3.1. The impacted member is tubular with the following data:

- Diameter D = 1m
- Thickness t = 25 mm

- Length L = 16 m
- Yield stress f_Y = 300 MPa
- Default hardening c = 0.002
- Axial springs in end 2 with stiffness 100 MN/m.

The beam is rotationally clamped so that it will start by developing a three hinge bending mechanism, where the bending action is transformed in membrane action when the deformations become finite. The axial springs delay the building up of axial force compared to fixed ends, and represents real conditions better.

The collision is run twice; 1st using the BIMPACT input option and local denting is included, 2nd applying a concentrated force at mid span, and local denting is not included.

The collision case corresponds to a kinetic energy of 10 MJ.

The results are shown in Figure 3.19through Figure 3.21.

The global load versus global displacement in Figure 3.20 shows how the local dent in the middle of the beam reduces the capacity of the beam, especially in the bending regime.

The bending moment in the middle of the beam with local denting is significantly smaller than that without denting, refer Figure 3.20. The difference increases with increasing deformations because the dent depth increases. However, the bending moment is also reduced by the increase of the axial force.

The strain histories versus global displacement with or without dent are plotted in Figure 3.21 along with the dent depth. The maximum strain occurs at beam ends when local denting is included at mid span, but are approximately equal at beam ends and mid span when denting is not included.

The strain at mid span is relatively small, because the reduced effective diameter reduces the bending induced strains. The local denting does however, also affect the strain at beam ends; because of the reduced bending moment at mid section, the effective cantilever length for the end hinge increases, and hence, the strains become smaller.

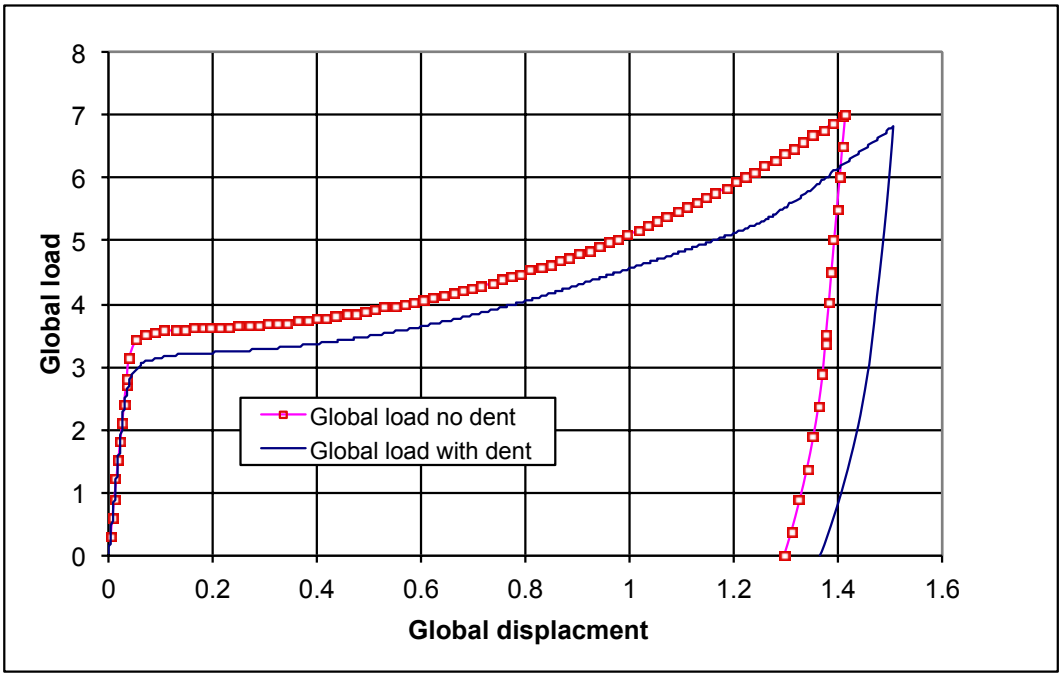

Figure 3.19 Global load versus global displacement

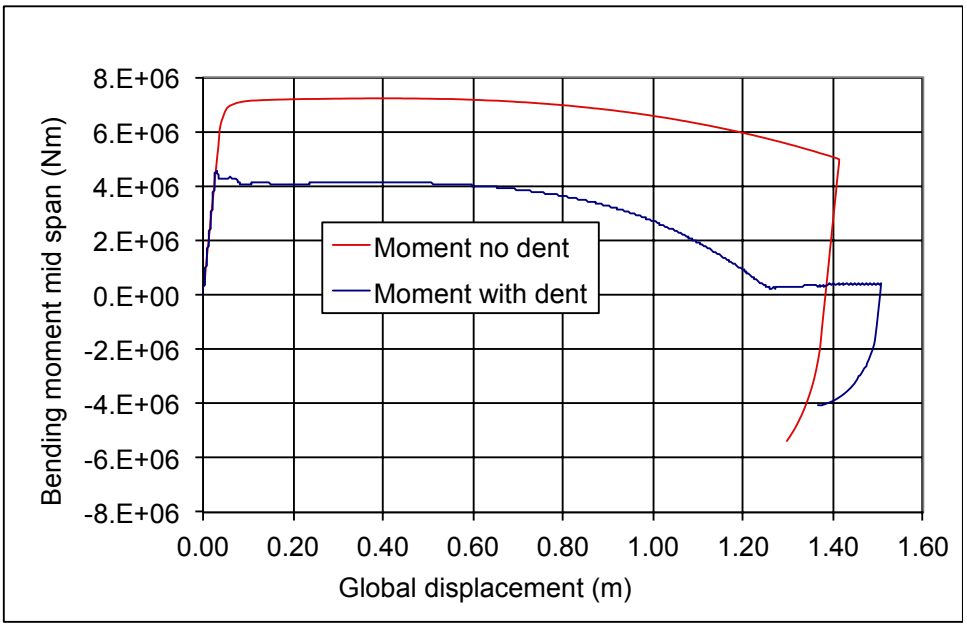

Figure 3.20 Mid span bending moment versus global displacement

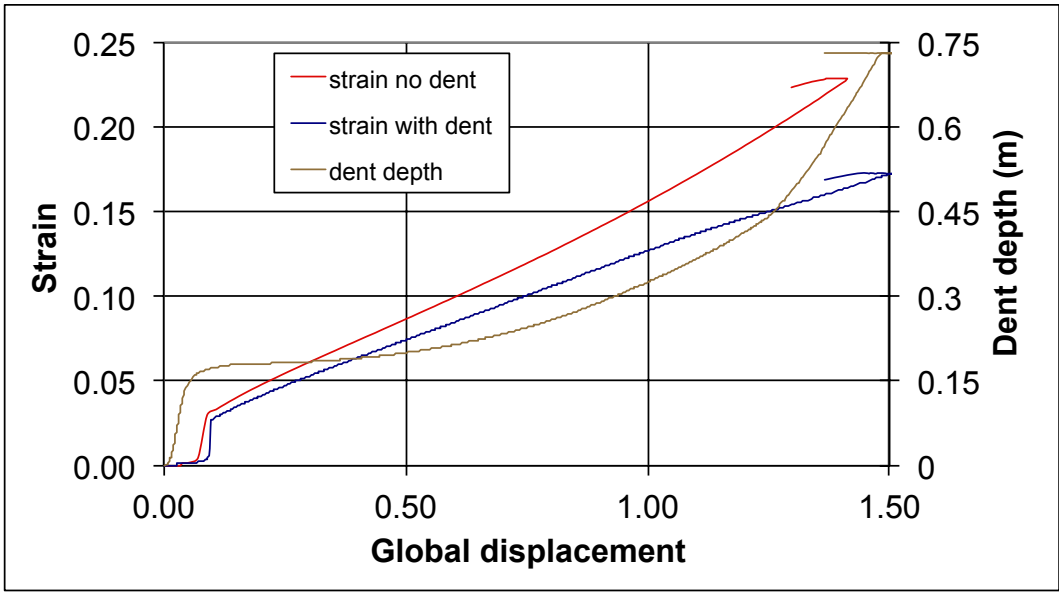

Figure 3.21 Strain and dent depth versus global displacement

4 Determination of strain model parameters.

Two important effects influence the assessment of strains in the plastic hinges:

1. The plastic rotations and plastic axial displacements calculated in Usfos. These do in turn depend on the hardening values used in the Usfos material model (refer c-factor in MISOIEP, MONPLAS etc)
2. The strain hardening parameters in the strain calculations routine

In the present version of Usfos the strain hardening parameters in the response analysis and the strain calculation model are not directly related.

The default strain hardening model in USFOS is uses a hardening coefficient $c_h = 0.002$. This factor is applied on all stress resultants (Note that in principle the strain hardening value for bending should not be exactly equal to the strain hardening in axial tension/compression. This effect is of little importance and is disregarded). The default value is conservative, and gives slightly too large plastic rotations and displacements.

According to Norsok N-004 the hardening values and critical strains for the three steel grades in Table A.3-4 may be used. It is observed that most values differ from the default values in Usfos.

Table A.3-4 Proposed values for e_{cr} and H for different steel grades

Steel grade	ε_{cr}	H
S 235	20 %	0.0022
S 355	15 %	0.0034
S 460	10 %	0.0034

The present strain calculation model in Usfos has been based on the following default values:

$$\sigma_{ult} = 1.3\sigma_Y$$

$$\varepsilon_s = 20\varepsilon_Y \quad \varepsilon_Y = \frac{\sigma_Y}{E}$$

$$\varepsilon_{ref} = 0.15$$

On the basis of these default values stress strain curves for various grades are shown in Figure 4.1. The stress strain curves for strain calculation are defined up to a strain value of 0.15 regardless of the grade. Of course, a lower value may be chosen for the critical strain, but the full benefit of hardening is not appreciated. The present default values give a good stress-strain curve for grade S 355.

For grade S235 the hardening is "too fast" and for S460 "too slow". The yield plateau is also exaggerated for S 460

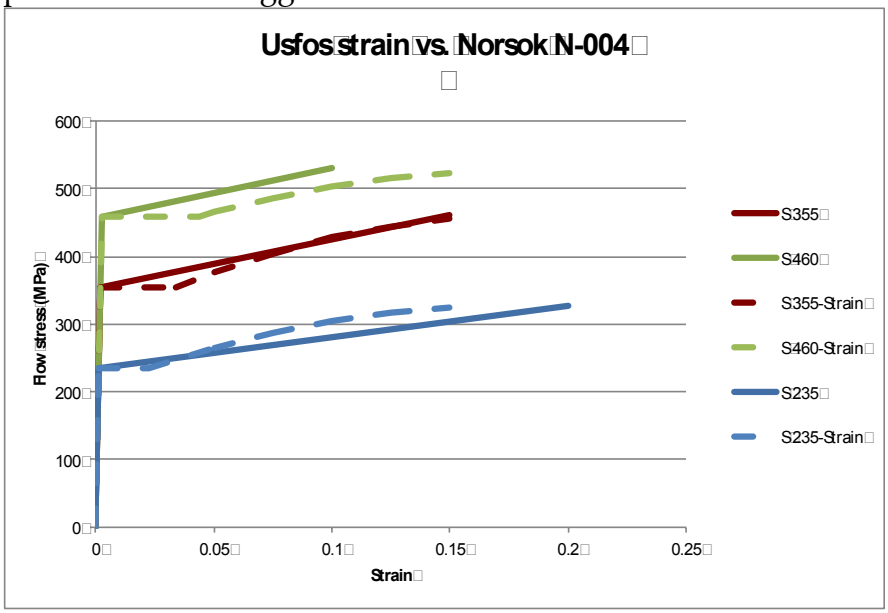

Figure 4.1 Stress strain relationships for original model (default values)

An alternative input model has been developed for grades between S 235 and S 460. In these cases the hardening parameters are assumed to follow those given in Norsok N-004 Table A.3-4. This gives:

<u>For grade S 235</u>

$$\sigma_{ult} = 1.39\sigma_Y = 327 \text{ MPa}$$

$$\varepsilon_s = 20\varepsilon_Y \quad \varepsilon_Y = \frac{\sigma_Y}{E} = 0.0011$$

$$\varepsilon_u = 0.20$$

$$\varepsilon_{ref} = \varepsilon_u - \varepsilon_s$$

For grade S 355

$$\sigma_{ult} = 1.30\sigma_Y = 461 \text{ MPa}$$

$$\varepsilon_s = 10\varepsilon_Y \quad \varepsilon_Y = \frac{\sigma_Y}{E} = 0.0017$$

$$\varepsilon_u = 0.15$$

$$\varepsilon_{ref} = \varepsilon_u - \varepsilon_s$$

For grade S 460

$$\sigma_{ult} = 1.15\sigma_Y = 530 \text{ MPa}$$

$$\varepsilon_s = 5\varepsilon_Y \quad \varepsilon_Y = \frac{\sigma_Y}{E} = 0.0022$$

$$\varepsilon_u = 0.10$$

$$\varepsilon_{ref} = \varepsilon_u - \varepsilon_s$$

The stress strain relationships for the strain calculations are illustrated in Figure 4.2. The flow stress coincides at the ultimate stress given in NORSOK. The parabolic stress-strain curve and the linear hardening curves deviate noticeably for intermediate strain values. However, this is of secondary influence; the most important parameter is by far the ultimate stress and this is attained for the critical stress.

Automatic calculation of NORSOK strain hardening parameters for strain calculations are offered in Usfos v8.6 for grades between S 235 and S 460. For intermediate values of the grades, linear interpolation is used. Refer Usfos release Notes v8.6 for details of input

For grades > S 460 no automatic calculation is offered. Appropriate value for the hardening parameter c_h remains the responsibility of the user.

Instead of using the default values or the automatic calculation for grades between S235 and S460, the user may specify all parameters for the strain-hardening model by means of the option "UserDef ". Refer Usfos release Notes v8.6 for details of input

If desired smaller values than those given in the NORSOK code may be used. This is conservative. The Usfos strain model is calibrated to give a good prediction for the acceptable strain levels given in NORSOK (i.e. strains in the range of 10%- 20%).

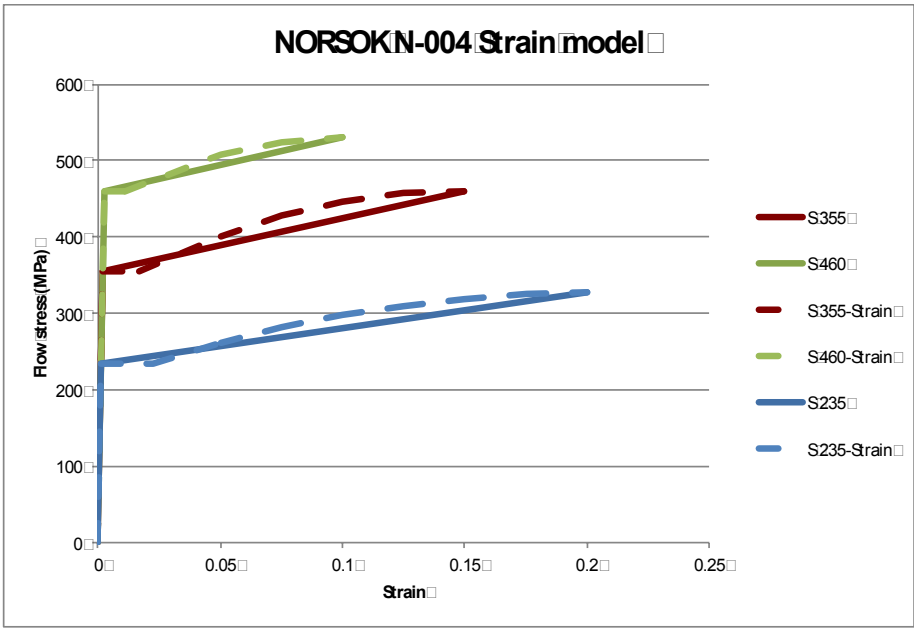

Figure 4.2 Stress strain relationships for revised model (key: S235,S355, S460)

REFERENCES

Skallerud B. and Amdahl, J., *Nonlinear Analysis of Offshore Structures* by Research Studies Press, 2002

a

Appendix: Excerpt from theory manual

10 FRACTURE CRITERIA

10.1 INTRODUCTION

Progressive collapse analysis by means of USFOS assumes implicitely perfectly ductile behaviour, i.e. rupture does not take place at any location. In practice the material endurance is limited, rupture may take place due to excessive straining possibly accelerated by local cracks. Hence, the capacity as predicted by USFOS may be overestimated.

An inherent problem with the plastic hinge concept used in USFOS is that no information is provided as to the strain level in the hinges. In fact, all strains are concentrated at one point of zero length, which means that the strains go towards infinity.

In order to develop a fracture criterion it is necessary to obtain a strain estimate. The purpose of the present study is to develop a simplified model, where the total strain is related to the plastic deformations in the yield hinge. The nominal strain is then compared with a critical strain derived from fracture mechanics principles (Level 3 method). If the critical strain is exceeded the member in question including its load effects should be removed in the subsequent analysis.

10.2 ROTATION IN ELASTO-PLASTIC REGION

10.2.1 Rectangular cross-section

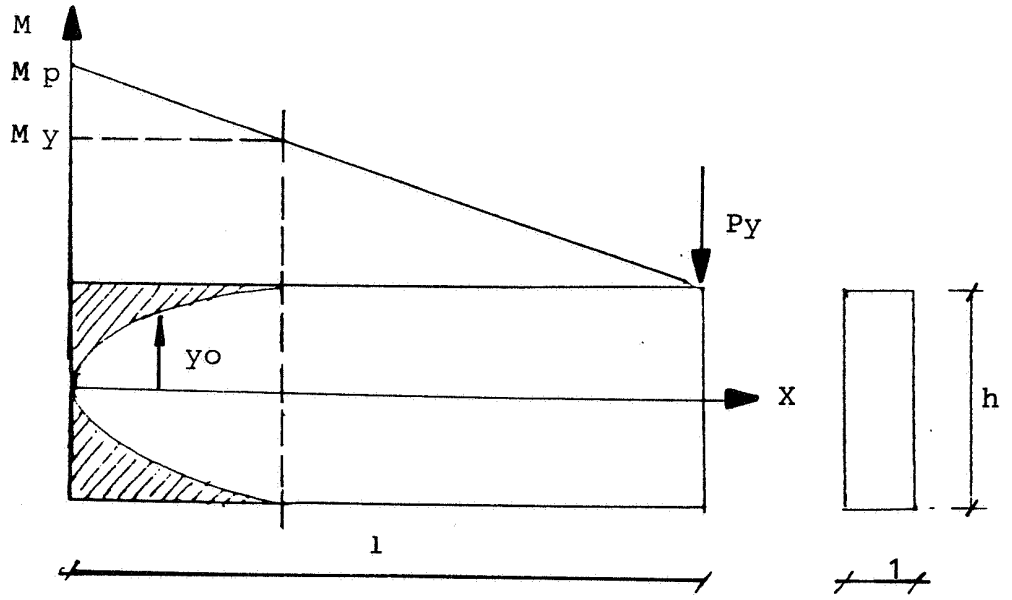

Figure 10.1 Cantilever beam

Consider the cantilever beam in Figure 10.1. The cross-section is elastic when $M < M_y$. Once $M = M_y$ yielding starts in the utmost fiber. For increasing bending moment the plastic zone spreads twoards the neutral axis. At the end the whole cross-section is plastified and the bending moment attains the plastic bending moment.

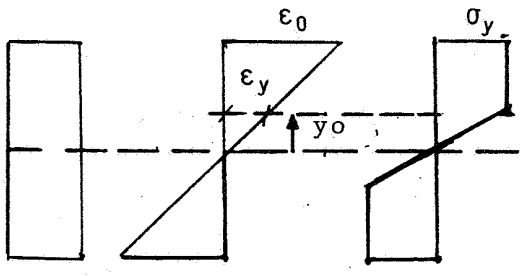

Figure 10.2 Strain distribution

The distribution of strain in the elasto-plastic section is sketched in Figure 10.2. When $\varepsilon_0 \geq \varepsilon_y$ the stress $\sigma = \sigma_y$ according to the assumption of linear elastic-ideal plastic behaviour. The corresponding moment is

$$M = 2 \int_0^{\frac{h}{2}} \sigma_y \, dy = M_p \left\{ 1 - \frac{4}{3} \left[\frac{y_0}{h} \right]^2 \right\} = M_p \left\{ 1 - \frac{1}{3} \left[\frac{\varepsilon_y}{\varepsilon_0} \right]^2 \right\} \qquad (10.1)$$

where

$$M_p = \frac{\sigma_y h^2}{4}$$

= the plastic bending moment for rectangular cross-section.

The axial variation of the bending moment is expressed as

$$M = M_p \left(1 - \frac{x}{l} \right) \qquad (10.2)$$

From Eq (10.1) and Eq (10.2) there is obtained

$$\frac{\varepsilon_0}{\varepsilon_y} = \frac{1}{\sqrt{3 \frac{x}{l}}} \qquad (10.3)$$

The rotation in the elasto-plastic zone from the onset of yielding to an arbitrary point, Δl, from the end is given by

$$\theta = \int_{\Delta l}^{l/3} \frac{2\varepsilon_o}{h} \, dx = \frac{2\varepsilon_y}{h} \int_{\Delta l}^{l/3} \frac{1}{\sqrt{3 \frac{x}{l}}} \, dx = \frac{4l\varepsilon_y}{3h} \left[1 - \frac{\varepsilon_y}{\varepsilon_{max}} \right] \qquad (10.4)$$

where ε_{max} denotes ε_0 at Δl.

This shows that the rotation in elasto-plastic zone for an ideal plastic material is bounded and approaches asymptotically the value

$$\theta_{ep} = \frac{4l\varepsilon_y}{3h} \qquad (10.5)$$

Conversely, the maximum strain can be estimated from the total rotation

$$\frac{\varepsilon_{max}}{\varepsilon_y} = \frac{1}{1 - \frac{3h}{4l\varepsilon_y} \cdot \theta} \qquad (10.6)$$

10.2.2 Tubular cross-section

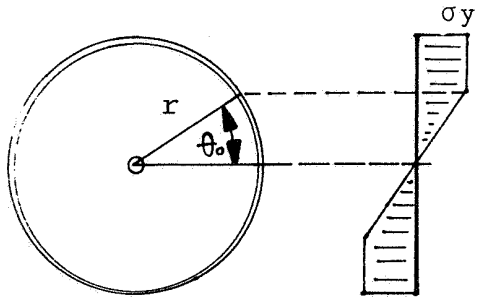

Figure 10.3 Stress distribution in tubular cross-section

Figure 10.3 shows the elasto-plastic stress-distribution in case of circular cross-section. The distance to the first yielding fiber is now described by the angle θ_0.

The corresponding bending moment is given by

$$M = M_p\left\{\frac{\theta_0}{\sin\theta_0} + \cos\theta_0\right\}/2 \qquad (10.7)$$

In the same manner as for rectangular cross-section the axial variation of the yield zone is determined by

$$\frac{\frac{\theta_0}{\sin\theta_0} + \cos\theta_0}{2} = 1 - \frac{x}{l} \qquad \frac{x}{l} < \{1 - \frac{\pi}{4}\} \qquad (10.8)$$

The total rotation can again be found by integrating the curvature in the elasto-plastic region

$$\theta = \int_{\Delta 1}^{(1-\frac{\pi}{4})1} \frac{\varepsilon_0}{r}\, dx \qquad (10.9)$$

A closed-form solution is difficult to obtain. Approximately, there is obtained

$$\theta = \frac{\varepsilon_y l}{2.3r}\left[1 - \frac{\varepsilon_y}{\varepsilon_{max}}\right] \qquad (10.10)$$

and

$$\frac{\varepsilon_{max}}{\varepsilon_y} = \frac{1}{1-\frac{2.3\ r}{\varepsilon_y l}\cdot\theta} \qquad (10.11)$$

10.3 ROTATION IN STRAIN HARDENING REGION

For large rotations strain hardening will occur. In the following the model shown in Figure 10.4 is used

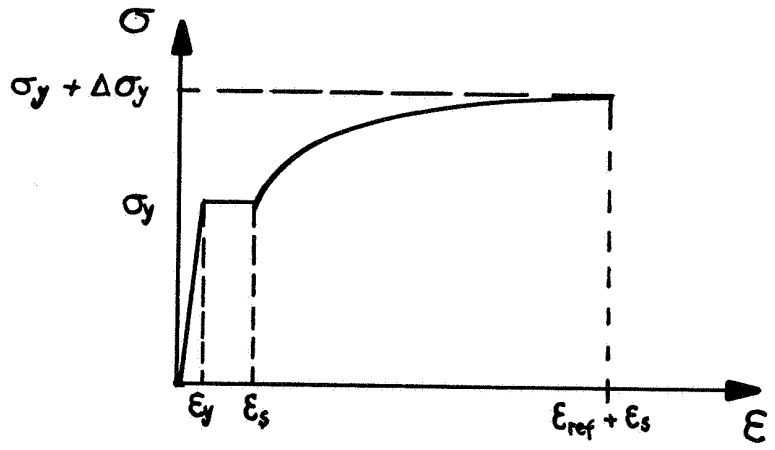

Figure 10.4 Strain hardening model

The yield strain is assumed constant in the range $\varepsilon_y < \varepsilon < \varepsilon_s$. For strains exceeding ε_s strain hardening takes place with a maximum value, $\Delta\sigma_y$, for $\varepsilon = \varepsilon_{ref} + \varepsilon_s$ where ε_{ref} signifies a reference strain. The hardening follows a parabolic relation given by

$$\Delta\sigma = \Delta\sigma_y \left[\frac{\varepsilon-\varepsilon_s}{\varepsilon_{ref}}\right]\left[2 - \frac{\varepsilon-\varepsilon_s}{\varepsilon_{ref}}\right] \qquad (10.12)$$

10.3.1 Bending

For a tubular cross-section the strain hardening contributes to the bending moment as illustrated in Figure 10.5.

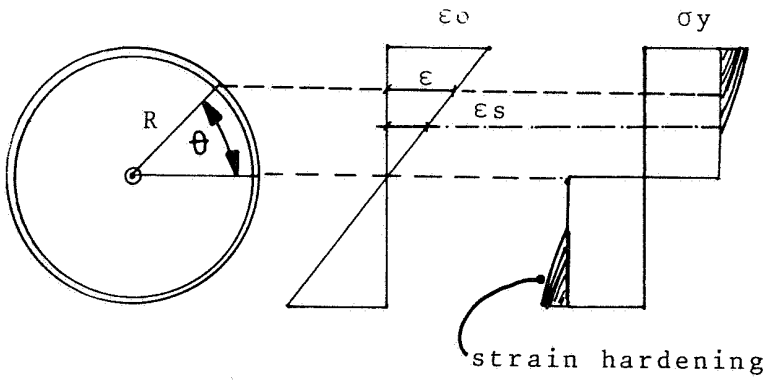

Figure 10.5 Strain/stress distribution for a tubular cross-section

The strain at an arbitrary fibre is given by

$$\varepsilon = \varepsilon_0 \sin\theta \tag{10.13}$$

where ε_0 is the maximum strain of the cross-section.

The additional moment due to strain hardening is now given by

$$\Delta M = 4r^2 t \Delta\sigma_y \int_{\arcsin \frac{\varepsilon_s}{\varepsilon_0}}^{\frac{\pi}{2}} \left[\frac{\varepsilon_0 \sin\theta - \varepsilon_s}{\varepsilon_{ref}}\right]\left\{2 - \frac{\varepsilon_0 \sin\theta - \varepsilon_s}{\varepsilon_{ref}}\right\} \sin\theta \, d\theta \tag{10.14}$$

$$= 4r^2 t \Delta\sigma_y \left\{\left[1 + \frac{\varepsilon_s}{\varepsilon_{ref}}\right]\frac{\varepsilon_0}{\varepsilon_{ref}}\left[\frac{\pi}{2} - \arcsin\frac{\varepsilon_s}{\varepsilon_0} - \frac{\varepsilon_s}{\varepsilon_0}\left[1 - \left(\frac{\varepsilon_s}{\varepsilon_0}\right)\right]^{1/2}\right]\right.$$

$$\left. - \frac{2}{3}\left[\frac{\varepsilon_0}{\varepsilon_{ref}}\right]^2\left[1 - \left[\frac{\varepsilon_s}{\varepsilon_0}\right]^2\right]^{3/2}\right\}$$

This can also be written

$$\Delta M = 4r^2 t \Delta\sigma_y \, f(\varepsilon_0) = 4r^2 t \Delta\sigma_y f(\varepsilon_{max}) \frac{f(\varepsilon_0)}{f(\varepsilon_{max})} \tag{10.15}$$

It is interesting to see that the maximum attainable moment is

$$\Delta M = 4r^2 t \Delta\sigma_y \left\{\frac{\pi}{2} - \frac{2}{3}\right\} = 3.62 r^2 t \Delta\sigma_y \qquad (10.16)$$

when $\varepsilon_s/\varepsilon_0 \rightarrow 0$, $\varepsilon_0/\varepsilon_{ref} \rightarrow 1$. The constant 3.62 is, as expected, higher than 3.14, corresponding to a linear stress distribution, but smaller than 4, corresponding to a uniform stress distribution over the cross-section.

For a cantilever, the bending moment varies linearly. Introducing a local coordinate system x at the point of strain hardening initiation, $f(\varepsilon_0)$ must obey the relationship

$$\frac{f(\varepsilon_0)}{f(\varepsilon_{max})} = \frac{x}{l_h} \qquad (10.17)$$

where l_n denotes the length of the strain hardening region.

The total rotation in the strain hardening region is

$$\theta_h = \int_0^{l_h} \frac{\varepsilon_0}{r}\, dx = \int_0^{l_h} \frac{1}{r} f^{-1}\left[f(\varepsilon_{max})\frac{x}{l_n}\right] dx \qquad (10.18)$$

It is very difficult to find closed form solutions to Equation (10.21) and approximate methods will be resorted to.

Rearranging, Equation (10.21) becomes

$$\theta_h = \frac{p\varepsilon_{ref} l_h}{r} \int_0^{l_h} \frac{1}{p}\left[\frac{\varepsilon_0 - \varepsilon_s}{\varepsilon_{ref}}\right]\frac{dx}{l_h} + \int_0^{l_h} \frac{\varepsilon_s}{r}\, dx \qquad (10.19)$$

where the parameter p is given by

$$p = \frac{\varepsilon_{max} - \varepsilon_s}{\varepsilon_{ref}} \qquad (10.20)$$

ε_{max} is the maximum strain occurring at the beam end. Figure 10.6 displays how the nondimensional strain is distributed over the strain hardening region.

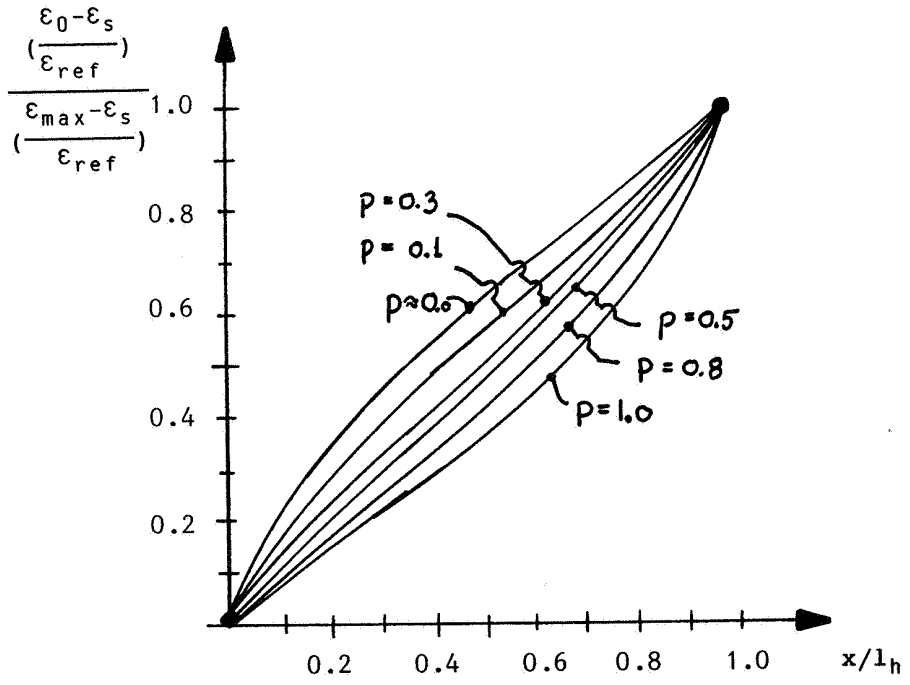

Figure 10.6 Strain distribution over hardening region

Relatively speaking, the strain intensity distribution is larger for moderate strain levels as compared with high strain levels.

A reasonable approximation to the integral in Equation (10.22) is offered by the expression

$$\int_0^{l_h} \frac{1}{p}\left[\frac{\varepsilon_0-\varepsilon_s}{\varepsilon_{ref}}\right]\frac{dx}{l_h} \approx \frac{1.2}{2+p} \qquad (10.21)$$

The length of the strain hardening region is found from

$$\frac{l_h}{l} = \frac{\Delta M/M_p}{1+\Delta M/M_p} = \frac{f(\varepsilon_{max})\cdot\frac{\Delta\sigma_y}{\sigma_y}}{1 + f(\varepsilon_{max})\frac{\Delta\sigma_y}{\sigma_y}} \qquad (10.22)$$

The relationship between $f(\varepsilon_{max})$ and p is shown in Figure 10.7.

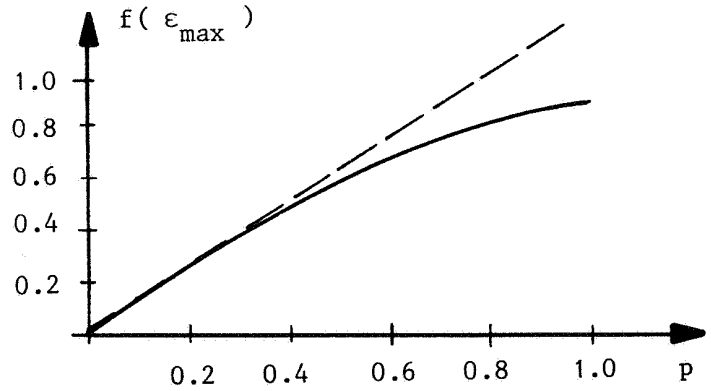

Figure 10.7 $f(\varepsilon_{max})$ versus the parameter p

The following approximation is introduced

$$f(\varepsilon_{max}) \approx \frac{1.4p}{1+0.5p} \qquad (10.23)$$

The rotation in the elastoplastic region is given by Equation (10.8)

$$\theta_{ep} \approx \frac{\varepsilon_y l}{2.3r} \qquad (10.24)$$

and

$$\frac{l_{ep}}{l} = \frac{1 - \frac{\pi}{4}}{1+f(\varepsilon_{max})\frac{\Delta\sigma_y}{\sigma_y}} = \frac{0.215}{1 + \frac{1.4p}{1+0.5p}\frac{\Delta\sigma_y}{\sigma_y}} \qquad (10.25)$$

Combining Equations (10.22, 10.24, 10.26, 10.27, 10.28) there is obtained

$$\theta = \theta_h + \theta_{ep} = \frac{\varepsilon_{ref} \cdot l}{r} \frac{1}{1 + \frac{\Delta\sigma_y}{\sigma_y} \frac{1.4p}{1+0.5p}} \left\{ \frac{1.2p}{2+p} \cdot \frac{\Delta\sigma_y}{\sigma_y} \frac{1.4p}{1+0.5p} + \frac{\varepsilon_s}{\varepsilon_{ref}} \cdot \frac{\Delta\sigma_y}{\sigma_y} \frac{1.4p}{1+0.5p} + \frac{\varepsilon_s}{\varepsilon_{ref}} \frac{\varepsilon_y}{\varepsilon_s} \frac{1}{2.3} \right\} \qquad (10.27)$$

Rearranging, there is obtained a second degree equation in p

$$ap^2 + bp + c = 0 \qquad (10.27)$$

where

$$a = 1.68 \frac{\Delta\sigma_y}{\sigma_y} + \left[1.4 \frac{\Delta\sigma_y}{\sigma_y} + 0.215 \right] \frac{\varepsilon_s}{\varepsilon_{ref}} - \frac{\theta r}{\varepsilon_{ref} l} \left[0.5 + 1.4 \frac{\Delta\sigma_y}{\sigma_y} \right] \qquad (10.28a)$$

$$b = \left[2.8 \frac{\Delta\sigma_y}{\sigma_y} + 0.86 \frac{\varepsilon_y}{\varepsilon_s} \right] \frac{\varepsilon_s}{\varepsilon_{ref}} - \frac{\theta_r}{\varepsilon_{ref} \cdot l} \left[2 + 2.8 \frac{\Delta\sigma_y}{\sigma_y} \right] \qquad (10.28b)$$

$$c = 0.86 \frac{\varepsilon_y}{\varepsilon_{ref}} - 2 \frac{\theta r}{\varepsilon_{ref} l} \qquad (10.28c)$$

Once p is solved the maximum strain is obtained from

$$\varepsilon_{max} = \varepsilon_{ref} \left[p + \frac{\varepsilon_s}{\varepsilon_{ref}} \right] \qquad (10.29)$$

10.3.2 Membrane Strain

The yield criterion formulated in terms of stress resultants takes the following form for a tubular cross-section

$$f(m, n) = 0 \qquad (10.30)$$

where $m = M/M_p$, $n = \pi/2\ N/N_p$ are nondimensional bending moment and axial force, respectively. The plastic increments in rotation and axial displacement are governed by the normality criterion, i.e.:

$$d\theta_p = d\lambda \frac{\partial f}{\partial m} \frac{\partial m}{\partial M} \tag{10.31a}$$

$$d\theta_p = d\lambda \frac{\partial f}{\partial n} \frac{\partial n}{\partial N} \tag{10.31b}$$

where $d\lambda$ is the plastic increment scalar. Combining, this yields

$$d\theta_p = \frac{\partial f/\partial m}{\partial f/\partial m} \cdot \frac{\partial m/\partial M}{\partial n/\partial N} du_p \tag{10.32}$$

and

$$d\theta_p = \frac{1}{\sin n} \cdot \frac{1}{r} du_p \tag{10.33}$$

This shows that the plastic axial displacement divided by the radius can be interpreted as an equivalent rotation. This corresponds to distributing the axial displacement over the effective hinge length. Hence, the total rotation to be used in Equation (10.31a-c) is

$$\theta^{tot} = \theta_p + \frac{u_p}{r} \tag{10.34}$$

The presence of axial force increases the effective hinge length as illustrated in Figure 10.8.

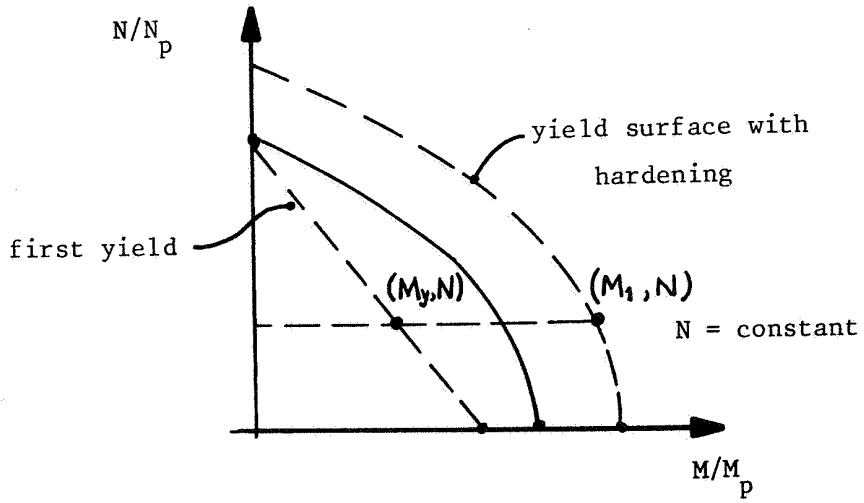

Figure 10.8 Axial force - bending moment interaction

The relative length of the plastic and elastoplastic zone is

$$\frac{l_{ep}}{l} = (1 - \frac{M_y}{M_1}) \tag{10.35}$$

Introducing the first yield Equation

$$\frac{4}{\pi}\frac{M_y}{M_p} + \frac{N}{N_0} - 1 = 0 \tag{10.36}$$

and the fully plastic surface

$$\frac{M_1}{(1+C_M)M_p} - \cos\frac{\pi}{2}\frac{N}{(1+C_N)N_p} = 0 \tag{10.37}$$

where C_M and C_N account for the hardening in the bending - and axial direction respectively. This gives

$$\frac{l_{ep}}{l} = 1 - \frac{\frac{\pi}{4}(1 - \frac{N}{N_p})}{(1+C_M)\cos\frac{\pi}{2}\frac{N}{(1+C_N)N_p}} \tag{10.38}$$

l represent the length from member end to the inflection point and is obtained from the formula

$$\frac{l}{l_{mem}} = \frac{1}{1 + \frac{M_2}{M_1}} \leq 1 \tag{10.39}$$

where l_{mem} is the total element length and M_2 denotes the bending moment at the opposite end.

Combining Equations (10.41 and 10.42) there comes out

$$\frac{l_{ep}}{l_{mem}} = \frac{1}{1 + \frac{M_2}{M_1}} \left(1 - \frac{\frac{\pi}{4}(1 - \frac{N}{N_p})}{(1+C_M)\cos\frac{\pi}{2}\frac{N}{(1+C_N)N_p}}\right) \qquad (10.40)$$

The augmentation of effective yield hinge length caused by the membrane force can then be obtained from

$$f = \frac{l_{ep}/l_{mem}}{l_{ep}/l_{mem}(N = M_2 = 0)}$$

$$= \frac{1}{1 + \frac{M_2}{M_1}} \cdot \frac{1}{1 - \frac{\pi/4}{1+C_M}} \cdot \left\{1 - \frac{\frac{\pi}{4}(1 - \frac{N}{N_p})}{(1 + C_M)\cos\frac{\pi}{2}\frac{N}{(1+C_N)N_p}}\right\} \qquad (10.41)$$

The bending parameter is taken as

$$C_M = f(\varepsilon_{max})\frac{\Delta\sigma_y}{\sigma_y} \qquad (10.45)$$

For simplicity C_N is chosen equal to C_m.